FRAMEWORK FOR MODELING POST-FIRE HYDROLOGY

WITH REMOTE SENSING

A Thesis

Presented to

The Faculty of the Department of Civil Engineering

California State University, Los Angeles

In Partial Fulfillment

of the Requirements for the Degree

Master of Science

in

Civil Engineering

By

Rafael Rodriguez

December 2022

The thesis of Rafael Rodriguez is approved.

Sonya R. Lopez, Committee Chair

Jingjing Li

Gustavo Menezes, Department Chair

California State University, Los Angeles

December 2022

ABSTRACT

Framework for Modeling Post-Fire Hydrology

with Remote Sensing

By

Rafael Rodriguez

As fire rages across a hillside, a hydrophobic layer is formed, which causes significant increases in the post-fire runoff by preventing water from infiltrating into the subsurface. Simultaneously, the loss of vegetation to fire can reduce water loss from groundwater because of reduced evapotranspiration. These effects can last for several years post-fire, depending on the fire intensity. This project aims to develop a fire-vegetation-hydrology model framework that explicitly considers the formation of a hydrophobic layer. The research team produced an automated "off the shelf" code that combines remote sensing products, including hourly meteorological (NLDAS-2), land cover (NLCD), topography (NED), and burn maps (BAER). This code produces the files necessary to run ParFlow-CLM, a 3D, parallel-processing, coupled land surface-groundwater hydrologic model, to simulate plant fluxes, surface fluxes, radiative fluxes, and variable saturation in the subsurface. Based on model results, this framework can be used by state, fire, and forest agencies to plan for post-fire remediation and strategically remove vegetation (fuel) between fires. Researchers will be able to test hypotheses of hydrophobic layer degradation and vegetation regrowth as well as assess the long-term impacts of wildfire on subsurface water storage, recharge of aquifers, and evaporation fluxes.

ACKNOWLEDGMENTS

This research was funded by the NSF grant to the CREST Center for Energy and Sustainability at California State University, Los Angeles (Award No. HRD-1547723) and the Graduate Equity Fellowship. Travel scholarships were provided by the Graduate Resource Center and the College of Engineering, Computer Science, and Technology at California State University, Los Angeles. Model simulations were processed on the NASADIRECT-STEM computing cluster at Cal State LA and the Extreme Science and Engineering Discovery Environment (XSEDE) Supercomputer at the University of California, San Diego (NSF Grant # ACI-1548562).

I want to thank my parents, Guadalupe and Hortensia Rodriguez, for making the sacrifice of leaving their homes and families behind to give me the opportunity of a better life. I would also like to thank my fiancé *Iliana* for believing in me and being in my corner every step of the way. Finally, I extend my deepest gratitude to my advisor Dr. Sonya R. Lopez, for the mental, scholarly, and emotional support through my 2.5-year program. Through long nights and plenty of hard work, I produced a thesis that I am incredibly proud of.

Estudia mucho mijo para que no tengas que trabajar toda la vida como un burro como yo.

-Guadalupe Rodriguez, 2007

TABLE OF CONTENTS

LIST OF TABLES

Table

LIST OF FIGURES

Figure

CHAPTER 1

INTRODUCTION

The United States is experiencing an increase in wildfire frequency and size (Westerling & Bryant, 2006); researchers expect this trend to continue as atmospheric temperatures rise due to human-induced perturbations (Kauffmann, Kauppi, Mann, & Stock, 2011). Air and soil moisture, temperature, fuel, and wind speeds are the main drivers of natural wildfires. Low moisture (soil and humidity) and high temperatures lead to drier vegetation. High winds may cause the fire to spread rapidly as wildfire begins. These factors lead to the development of "Megafires" that are highly catastrophic within California (Khorshidi et al., 2020). High-intensity wildfires create a variably thick water-repellent layer (or hydrophobic layer) within the first few centimeters of the soil (DeBano, 1968). This hydrophobic layer significantly contributes to infiltration-limited overland flow, and vegetation loss decreases evapotranspiration for several years during post-fire recovery (Kinoshita & Hogue, 2011). The fifth IPCC assessment report states that climate-related extremes, such as droughts and wildfires, will cause significant harm to sensitive ecosystems and damage human-made infrastructure (Team & Rajendra, 2014). IPCC researchers considered various fire regimes based on future climate projections; however, they did not evaluate the fire-vegetation dynamics, vegetation recovery, and their relationship to hydrologic components.

In addition to impacting water and vegetation, burned watersheds or burn scars are highly susceptible to catastrophic mass wasting events, also known as debris flows. These debris flows occur when storms reach hillsides with unconsolidated soil and ash above a hydrophobic layer. When a high-intensity storm hits a recently burned area, this ash layer can become mobile and form a debris flow (Cannon, Boldt, Kean, Laber, & Staley, 2010). This occurred in Montecito, CA, during the winter of 2017-2018. (USFS, 2018). The 280,000-acre burn scar from the Thomas Fire became saturated and unstable from the storms in Jan 2018. This mass wasting event caused twenty-three deaths and millions in damages.

Modeling natural phenomena inherently includes a level of generalization that must balance the oversimplification of the physical processes with the capabilities of the available software. One-dimensional models simplify three-dimensional problems by analyzing a single slice of terrain and subsurface. While these models can analyze physical processes through the subsurface profile, they assume all soil properties are isotropic, meaning that the soil properties are the same in every direction. This simplification doesn't account for preferential groundwater flux in any direction. Hydrus-1D, a one-dimensional surface-subsurface numerical model, was used to simulate vadose zone hydrology following the 2010 Fourmouline Canyon Fire in Colorado by Ebel, B.A. in 2013. While the 1D model could match observed conditions in north-facing slopes, it could not match the observed conditions in south-facing slopes. A more robust model would have been able to compare all observed trends. Watershed management agencies often focus on changes to hillside peak flows and the probability of debris flows after a fire occurs in their management area.

Watershed routing models such as Hydrologic Engineering Center Hydrologic Modeling System (HEC-HMS) use synthetic precipitation events and surface parameters (runoff coefficients and infiltration rates) to calculate hydrographs indicating the peak flow rates for each storm event. Cydzik and Hogue (2009) modeled post-fire flooding with HEC-HMS. However, their model outputs were limited to points on open channels.

ParFlow-CLM was used by Atchley et al. (2018) to simulate a pre- and post-fire distributed hydrological model at a hillslope scale (1000 m^2) with varying degrees of evapotranspiration loss. They model a homogeneous burn severity in each post-fire scenario by reducing the leaf area index (LAI) and saturated hydraulic conductivity in the top two centimeters of soil. Escobar-Sanchez (2020) advanced the state of the science by conducting a sensitivity analysis of heterogeneous burn severity at a larger scale (500,000 m^2) by spatially varying changes to saturated hydraulic conductivity, LAI, and burn depth. Their work simplified the topography to model simplified hillsides with a constant slope throughout the model domain. Our work strives to extend the work pioneered by Escobar-Sanchez to the watershed scale with the natural topography and to create a framework for future researchers to create and run these complex models efficiently.

The four goals of this research are 1) to develop an off-the-shelf modeling framework accessible to researchers with little to no modeling expertise, 2) explicitly consider the hydrophobic layer formation; 3) to use open-access satellite observations to inform the model, and 4) provide a time-saving and efficient model set-up. The team built a series of processing scripts to extract and format the raw data into the appropriate files used to run ParFlow-CLM models representing hydrologic conditions before and after the wildfire event. Hydraulic properties can each be individually controlled and spatially varied within our package in the setup of a ParFlow-CLM model, making it an appropriate pairing to study the hydrology of burn scars after wildfires ravage a hillside. The team built the processing scripts to target the specific formats of NLDAS, BAER, NED, and NLCD data. These open-source databases can be used freely and easily accessed by future researchers to model scenarios past the publication of this report. Within minutes, the code developed by this team can process and synthesize the files required to model a year-long scenario that spans over 1,000 km^2. The final product is a package that contains the raw data files and the MATLAB scripts required to extract and format the scripts. This package will be available to any researcher interested in hydrologic modeling.

CHAPTER 2

Materials and Methods

ParFlow-CLM

The research team used ParFlow-Common Land Model (PF-CLM) to run hydrologic simulations of pre- and post-fire scenarios. This coupled model framework simulates surface water-groundwater hydrologic interactions (Maxwell, 2013; Kollet & Maxwell, 2008; Maxwell & Kollet, 2006; Maxwell & Miller, 2005; Woodward & Jones, 2001; Ashby & Falgout, 1996). ParFlow (PF) calculates subsurface variable saturation using the three-dimensional Richards equation (Equation 2.1) and surface water (overland) flow using the two-dimensional Manning's equation with kinematic wave approximation (Equation 2.2). The Common Land Model (CLM) is a land surface model that simulates land-atmosphere fluxes such as evapotranspiration (ET) using ground-atmosphere observations. CLM calculates transpiration fluxes from plants and evaporation fluxes from the ground and root zone (Dai, et al., 2003). Figure 1 visualizes the coupling of the ParFlow and CLM models.

$$S(p)S_s\frac{\partial p}{\partial t} - \frac{\partial(S(p)\rho(p)\phi)}{\partial t} - \nabla\cdot(\mathbf{K}(p)\rho(p)(\nabla p - \rho(p)\vec{g})) = Q, \text{ in } \Omega \tag{2.1}$$

$$v_x = -\frac{\sqrt{S_{f,x}}}{n}\Psi_s^{\frac{2}{3}} \quad , \quad v_y = -\frac{\sqrt{S_{f,y}}}{n}\Psi_s^{2/3} \tag{2.2}$$

In equation 1, per the ParFlow manual, Ω is the flow domain, p is the pressure head of water [L], S is the water saturation, S_s is the specific storage coefficient [L^{-1}], Φ is the porosity of the porous medium, ***K(p)*** is the hydraulic conductivity tensor [LT^{-1}], and Q is the water source/sink term [L^3T^{-1}]. The variables in equation 2.2 are as follows: v_i is the depth-averaged velocity vector [LT^{-1}], $S_{f,i}$ is the friction slope, i stands for the x- y- direction, n is the Manning's coefficient [$TL^{-1/3}$], and Ψ_s is the vertically averaged surface pressure (Maxwell R. , et al., 2019).

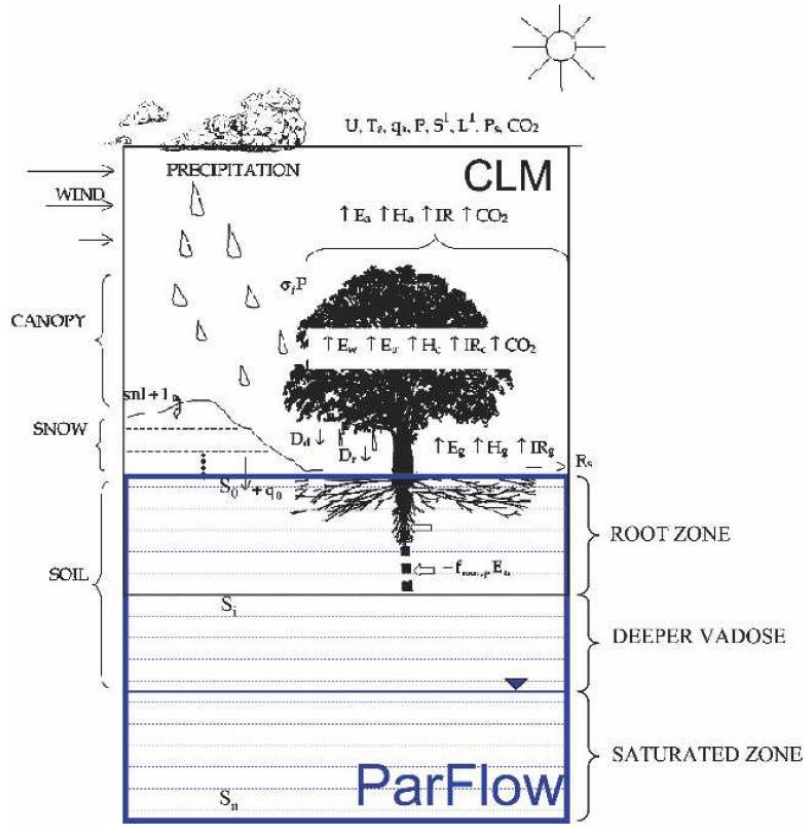

Figure 1. Coupling of ParFlow and CLM models from Maxwell and Miller 2004.

ParFlow-CLM uses a defined cell width, depth, height (DX, DY, and DZ), and the number of cells in each dimension (NX, NY, and NZ) to simulate a three-dimensional computational domain. Each cell in the domain is assigned physical properties, including saturated hydraulic conductivity (K_{sat}) and porosity (Φ). These parameters are used to calculate changes in hydrologic conditions over time. The matrix can be configured to represent a hillside, watershed, state, and even the contiguous United States (Condon & Maxwell, 2015). The number of processors and computing time available limits the domain's extent and resolution. The finer the resolution and broader the spatial domain, the more computational cells are necessary; thus, more computations are required per time step. The parallel processing capabilities of the model allow for the distribution of the computing load across multiple processors in a computing cluster, as demonstrated in this project.

CLM uses the International Geosphere Biosphere Programme (IGBP) classifications to describe eighteen biome types. Each biome type has nineteen physical parameters (i.e., minimum and maximum leaf area index, aerodynamic resistance, etc.) that are used to calculate evaporation from the surface, evapotranspiration from the root zone, open canopy, and total evapotranspiration from a domain. See Table 1 for the complete list of CLM variables.

Table 1. Common Land Model Parameter Description

CLM Variable	Description
itypwat	1-soil, 2-land ice, 3-deep lake, 4-shallow lake, 5-wetland: swamp, marsh
lai	Maximum leaf area index [-]
lai0	Minimum leaf area index [-]
sai	Stem area index [-]
z0m	Aerodynamic roughness length [m]
displa	Displacement height [m]
dleaf	Leaf dimension [m]
roota	Fitted numerical index of rooting distribution
rootb	Fitted numerical index of rooting distribution
rhol_vis	Leaf reflectance visible
rhol_nir	Leaf reflectance near-infrared
rhos_vis	stem reflectance vis
rhos_nir	stem reflectance nir
taul_vis	leaf transmittance vis
taul_nir	leaf transmittance nir
taus_vis	stem transmittance vis
taus_nir	stem transmittance nir
xl	leaf/stem orientation index
vw	btran exponent

Satellite Datasets

The hourly meteorological data required to run ParFlow-CLM was air temperature [K], specific humidity [kg/kg], surface pressure [Pa], eastward wind component [m/s], northward wind component [m/s], longwave radiation [W/m^2], shortwave radiation [W/m^2], and total precipitation [mm/s]. This data was sourced from the Phase 2 North American Land Data Assimilation System (NLDAS-2) at a 0.125°x0.125° (~ 13.875 km x 13.875 km) spatial resolution (Xia, et al., 2012). NLDAS-2 covers the entire continental United States and extends from 25° to 53° Latitude and from -125° to -67° Longitude. NLDAS-2 combines satellite data, radar precipitation measurements, and precipitation gauge observations to form land surface forcing model datasets. These datasets are spatially extrapolated to the finer resolution of the NLDAS-2 grid and temporally interpolated to an hourly time step (Xia et al., 2012). The research team employed a similar workflow to sort the various inputs into standardized units, cell size, and matrix origin.

We differentiated between pre- and post-fire conditions by simulating a change in saturated hydraulic conductivity (K_{sat}). Fire severity is correlated with hydrophobic layer formation, which is a critical factor in determining the change to runoff, erosion, and vegetation recovery (Keeley, 2009). Fox et al. (Fox, 2007) found that saturated hydraulic conductivity increases with increasing soil particle size distribution and decreases post-fire based on burn severity. To account for this, we used an empirical equation to determine saturated hydraulic conductivity based on the Difference Normalized Burn Ratio (dNBR) as done by Atchley et al. (Atchley, 2018). Normalized Burn Ratio (NBR) uses the ratio between near-infrared (NIR) and shortwave infrared (SWIR) to note the health of vegetation in each area (Miller & Thode, 2007). To account for variations in vegetation type, the difference in pre- and post-fire NBR is used to estimate burn severity; the difference is referred to as dNBR. The higher the dNBR, the higher the burn severity (Keeley, 2009).

Test Study Area

We identified the 2020 August Fire as an ideal test study area. The fire occurred in August of 2020 and burned over one million acres and spanned seven northern California counties near the Mendocino National Forest. The fire started on 8/16/2020 by lightning strikes and was contained on 11/11/2020. The burnscar spanned from 39.4° N, -123.5° E to 40.4° N, -122.5° E.

Figure 2. Test Study Area

The team focused on a portion of the burnscar near a reservoir to have in-situ water level data that can be used to calibrate the model in later efforts. The chosen extents were: 40.0608° N, -123.4569° E – 40.3860° N, -123.1064° N. The cell dimensions for the model were 30m x 30m x 1 m in the x, y, and z directions. The number of cells in the x, y, and z directions were 464, 224, and 10, respectively. This resulted in a total of 1,039,360 cells in the computational matrix. The discretization of this matrix is described in the pre-processing and processing sections below.

Pre-processing

The deliverable from this research project is a MATLAB package that can produce ParFlow-CLM run files to model pre- and post-fire conditions for the 2020-2021 fire season. Before executing the MATLAB code, the research team had to synthesize, edit, and format the raw input files using ArcGIS Pro version 2.9.3 (ESRI, 2011). Namely, four geospatial datasets needed to be uniformly formatted. These inputs included (1) meteorologic forcing from NLDAS, (2) burn severity raster files from the

United States Geological Survey (USGS) Burned Area Emergency Response (BAER) Imagery Support Program (USGS, 2020), (3) digital elevation models (DEM) from the National Elevation Dataset (United States Geologic Service, 2018), and (4) land cover distribution from the North American Land Change Monitoring System (NALC; (North American Land Change Monitoring System, 2015)). A visualization of the four significant inputs proceeding through the pre-processing workflow is shown in Figure 3.

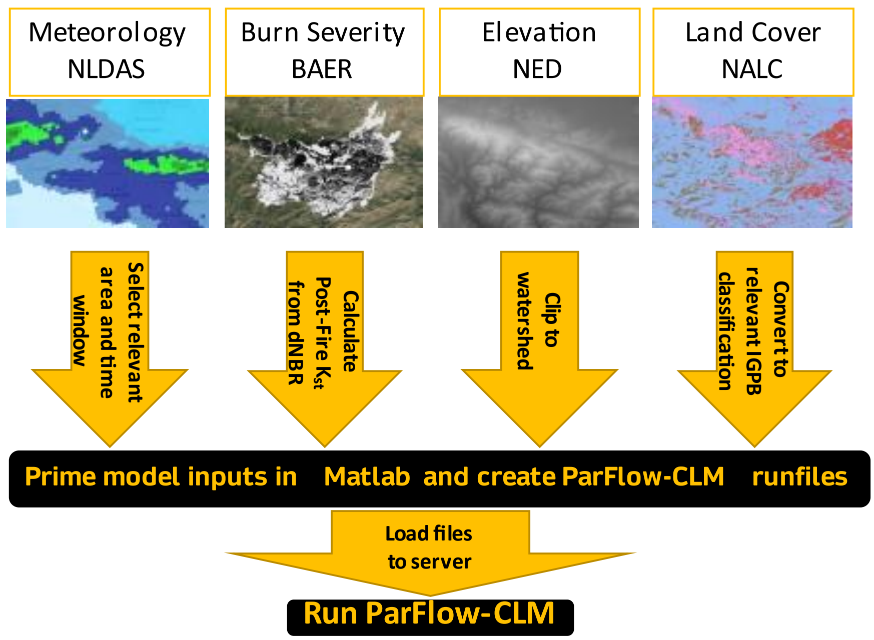

Figure 3. Pre-processing workflow

The research team gathered national, hourly meteorologic data (NLDAS) from January 1st, 2020 – December 31st, 2021. Each NLDAS time step contained all eleven variables for each of the 103,936 cells in the 464 (longitude) x 224 (latitude) grid. Two years of NLDAS data required over 2.2 GB of storage. This dataset was archived and processed in MATLAB, as described in the MATLAB section below.

We extracted burn severity maps for California spanning 2015 to 2021 from the United States Geologic Survey (USGS) Burned Area Rapid Response (BAER) website

(USGS, 2020). These burn severity maps show the severity and extent of fire damage within each burned area or burn scar. This portal provided raw dNBR values, which were converted to saturated hydraulic conductivity (K_{sat}) using Equation 2.3. Note that it differs from that presented in the literature (Atchley, 2018). The formula presented had the first constant defined as 390. However, when the team tried to apply this formula to dNBR datasets, the resulting K_{sat} values were higher than expected by a few orders of magnitude. The team then looked at the supplemental tables provided in the paper. It concluded that there was a typographical error in the transcription of the formula used to convert dNBR to K_{sat}.

$$K_{sat} = 0.39 * \exp(-0.0056\ dNBR) \tag{2.3}$$

Once the dNBR values were converted to K_{sat} values for each burn scar, the processed rasters were clipped to burn extents and mosaiced into a single raster; we placed -9999 in cells where there were no burn scars present. This K_{sat} raster was in a UTM 10N coordinate system and had a 20-meter by 20-meter resolution.

We downloaded LiDAR data for all fifty-eight counties in the state of California. The LiDAR dataset was in the UTM 10N coordinate system and had a 30-meter by 30-meter resolution. We used the LiDAR dataset to extract the digital elevation map (DEM), and it was merged into a single cohesive TIFF file for the state.

Land coverage data was downloaded from the North American Land Change Monitoring System (NALC; North American Land Change Monitoring System,2015). This land cover was classified into nineteen vegetation types, while the International Geosphere Biosphere Programme classification system used by CLM only used eighteen. The land cover was reclassified according to the same method implemented by Condon

(2015). This land cover raster file was in the World Geodetic System 1984 (WGS 84) coordinate system and had a 30-meter by 30-meter resolution.

The input data sets had varying coordinate systems, the most common being in World Geodetic System 1984 (WGS 84) and Universal Transverse Mercator (UTM). The WGS 84 coordinate system provides spatial location based on latitude and longitude, while UTM uses meters. Due to the earth's curvature, UTM is a projection of spherical latitude and longitude coordinates to sections of rectangular coordinates that conform to a grid. The section used in California is UTM 10N. The cell size for each raster was determined by converting a 30-meter by 30-meter raster from UTM 10N to WGS 84 and using the given cell size in degrees. The rasters were clipped to the same extent to maintain the same origin point for each matrix.

When reading the data sets into MATLAB, the elevation, saturated hydraulic conductivity, and landcover rasters maps were converted into two-dimensional matrices visualized as a table with 1094 columns and 1015 rows. Forcing the rasters into the same coordinate system, cell size, and origin ensured that MATLAB could overlay the matrices to extract the appropriate data, as the code would look for data at the same column and row number.

MATLAB Processing

The team produced a MATLAB script for processing the terrain, land cover, meteorology, and saturated hydraulic conductivity information into the format required for ParFlow-CLM to run successfully. This code is structured into the main script that hosts the user-defined inputs and calls on fourteen subscripts, one for each subroutine. The user-defined inputs include spatial limits, model resolution, temporal limits, temporal resolution, hydraulic parameters, soil type, file paths, and folder names. The fourteen subscripts execute tasks including importing, clipping, formatting, georeferencing, calculations, conversions and synthesizing. Table 2 lists the user-defined variables, descriptions, and default values.

The following section outlines the steps necessary for the user to run the script package built by the research team. First, the user downloads the file package that contains the MATLAB scripts and preprocessed data files. Upon opening the MATLAB script, the user is prompted to enter minimum and maximum latitude and longitude coordinates. The horizontal spatial resolution (30m x 30m) was predetermined by the resolution of the input datasets and is currently not a parameter the user can change. The user sets the vertical resolution and depth of the model. The team initially used the general vertical discretization (DZ) of 1 meter and NZ as ten layers creating a total domain depth of 10 meters.

The script 'create_variableDZ.m' in the script package specifies variable thickness of the burned and unburned layers. The uppermost layers of the matrix produced by the MATLAB script are defined as the burn layers. The variable *nlayers* defines the number of layers to be modeled as the depth of the burn penetration. Four burn layers were used in the example model at a thickness of 0.025m each. The rest of the soil thickness is split between the remaining unburned layers. The MATLAB script uses heterogenous K_{sat} values for the burn layers and homogeneous K_{sat} values for the nonburn layers.

Table 2. MATLAB User-Defined Variables

	Variable Name	Description	Class	Default Values
1	runname	File Name	String	testrun
2	predir	Server Directory	String	/home/rrodri144/Research/ Parflowrun
3	latmax	Maximum Latitude	Double	40.3860
5	latmin	Minimum Latitude	Double	40.0608
6	lonmin	Maximum Longitude	Double	-123.4569
7	lonmax	Minimum Longitude	Double	-123.1064
8	dx	Cell Width	Integer	30
10	dy	Cell Height	Integer	30
11	dz	Cell Depth	Integer	1
12	nz	Number of Vertical Layers	Integer	10
14	nlayers	Number of Burn Layers	Integer	4
18	xlower	Lower Piezometric Head Limit	Double	3
20	xupper	Upper Piezometric Head Limit	Double	12.4
21	drv_clmin_restart	Starting with Restart File?	Integer	2
24	ICPressurevalue	Initial Pressure	Double	0.0
25	mannings_u	Manning's n for Unburned Surface	Double	0.035
26	mannings_b	Manning's n for Burned Surface	Double	0.02
28	specificstor_u	Specific Storage for Unburned Surface	Double	1.0e-5
30	specificstor_b	Specific Storage for Burned Surface	Double	1.0e-5
32	dump	Output Interval	Integer	-1
33	startdate	Start Date	Date	01/03/2021
35	enddate	End Date	Date	01/10/2021
36	SubSoil_Depth	Soil Depth	Integer	10
38	Soil_Type	Soil Type	String	SANDY LOAM
43	indname	Indicator File Name	String	INDICATORFILENAME.pfb
44	rootdir	Local Directory	String	C:/Users/rodri/Documents/ Cal_State_LA/ParFlow/ Research
47	OutputFolderName	Output Folder Name	String	Parflowrun
48	OutDir	Output Directory	String	[rootdir,'/Parflowrun/']

The user defines the initial piezometric head, manning's surface roughness, and specific storage pending general knowledge of the surface and groundwater conditions. The user is prompted to select the soil type for the model domain. Based on the soil type hydraulic conductivity, porosity, and van Genuchten parameters as defined in the Gleeson Table (Gleeson, et al., 2011).

Finally, the user shall specify the name of the model run (*runname)* and the host directory for the raw input files and output runfiles *(Outdir).*

A detailed visualization of the workflow shown in Figure 3 is expanded in Figures 4-7. Figure 4 shows the workflow and steps necessary to clip and process the DEM. Figure 5 shows the clipping and formatting of the landcover data. Here, the schematic shows that there is X and Y data associated with each row in the final format. This is consistent with the formatting required by CLM. Figure 6 shows the clipping and formatting of the NLDAS forcing data. Figure 7 shows the steps and combination of saturated hydraulic conductivity in the format required by ParFlow-CLM. Table 3 describes each subscript and follows the workflow shown in Figures 4-7.

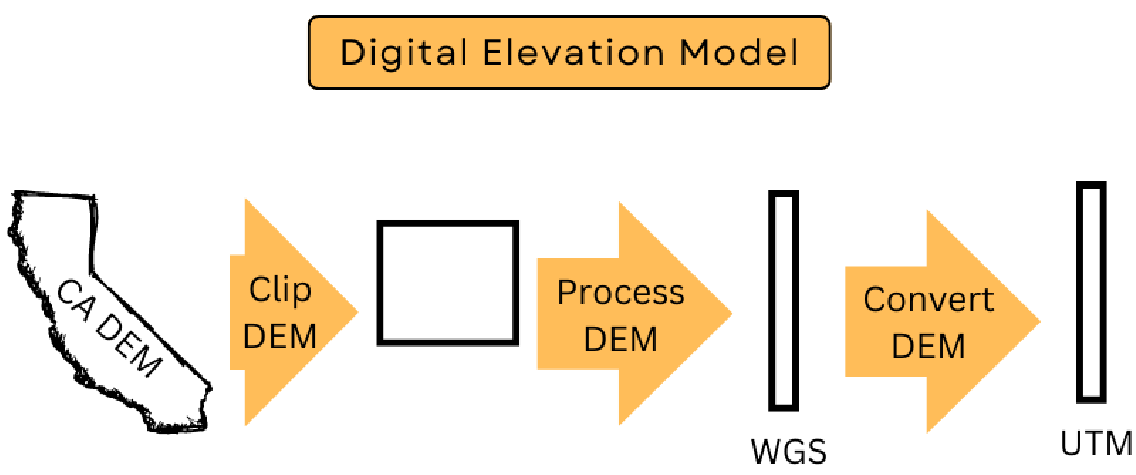

Figure 4. DEM processing

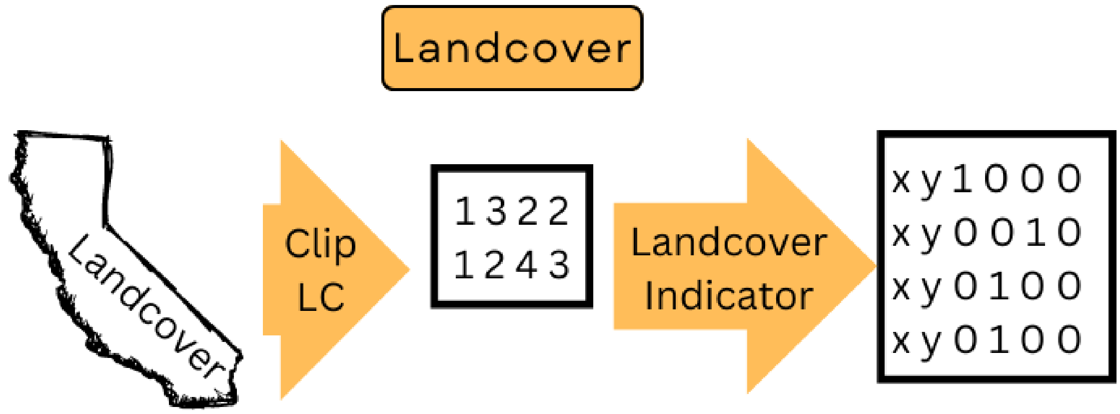

Figure 5. Landcover Processing

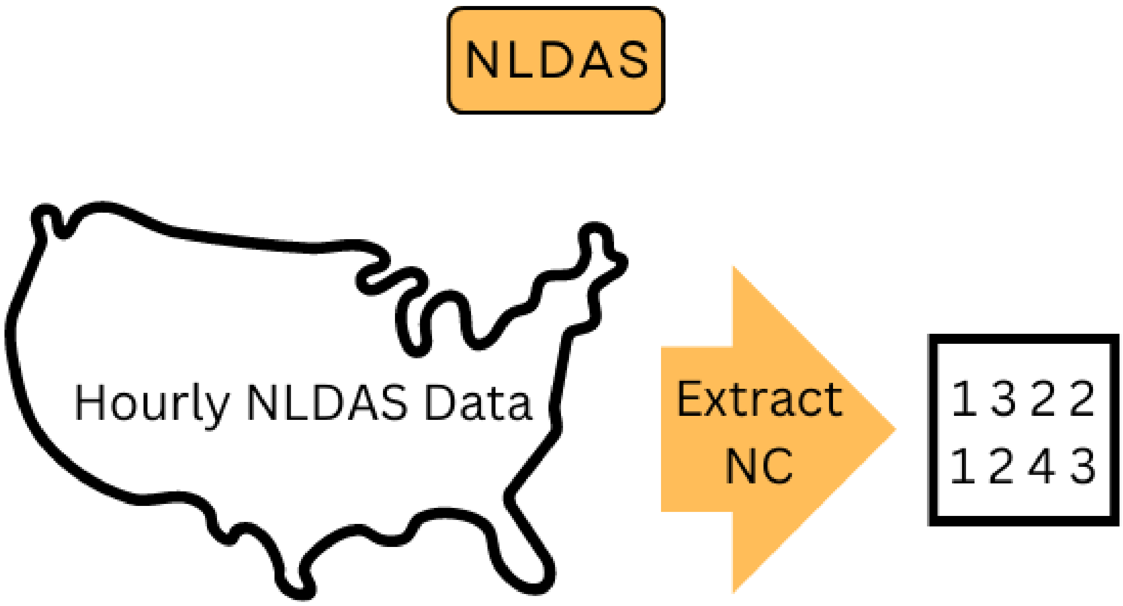

Figure 6. NLDAS Processing

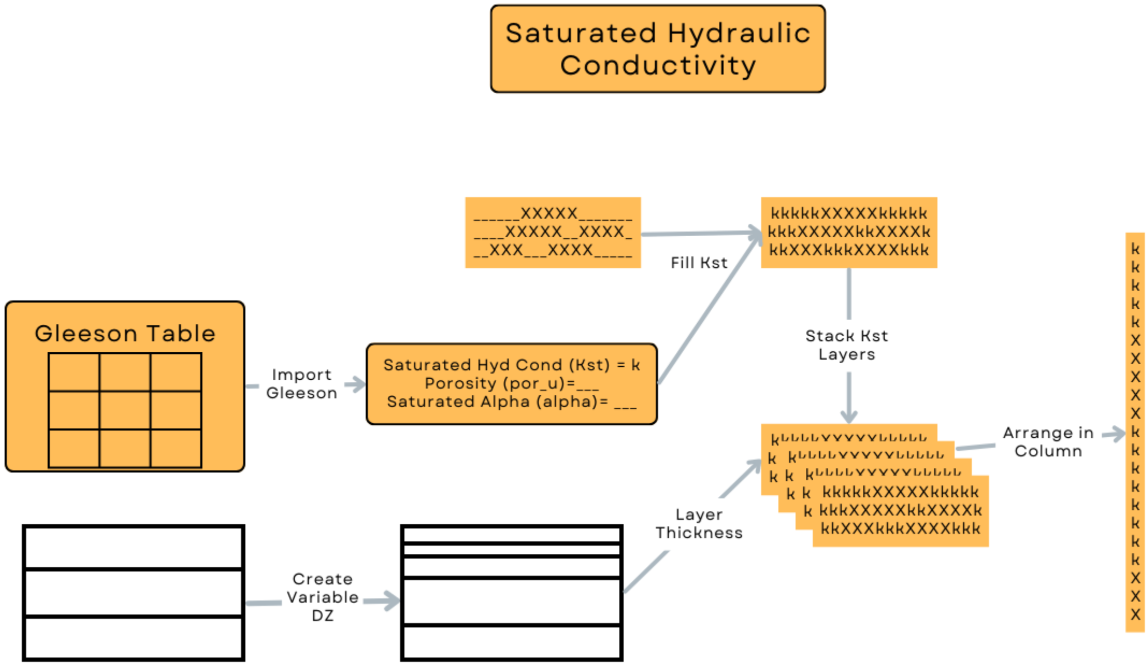

Figure 7. Saturated Hydraulic Conductivity Processing

CHAPTER 3

Results

MATLAB

The MATLAB package can process the topographic, burn severity, atmospheric forcings, and land cover data sets into the appropriate run files in 282.8 seconds or just under 5 minutes. Once the runfiles are compiled a researcher can start the ParFlow-CLM model with minimal effort. Table 3 lists the name, function summaries, and run times for each subscript included in the MATLAB package. Notably, reformatting the land cover data took nearly half of the entire runtime. The next longest time sink is the Burnscar.m subscript. This subscript replaces null K_{sat} values with the K_{sat} values from the Gleeson Table and then builds the 3-dimensional matrix by stacking 2-dimensional layers at the appropriate thickness.

ParFlow-CLM

Once the runfiles are compiled in MATLAB, the researcher can launch the model run in ParFlow-CLM. The team had access to a computer cluster allowing for selecting the number of processors used for each run. The team chose to run a one-year simulation using 16 processing cores divided by 4 for the x direction and 4 for the y direction. Among many output variables, three hydrologically significant outputs are Surface Storage, Subsurface Storage, and Surface Runoff. They indicate the amount of water stored on the surface, in the ground, and running off the surface.

Figure 8 shows the graphs of these three variables over time. Surface storage and runoff don’t rise until the subsurface is saturated near hour 200. This can be explained as the spin-up time required for the model to reach the initial equilibrium. This spin-up time may vary with the model domain and time span chosen.

The runoff graph in Figure 8 shows that the model starts to reach hydrologic equilibrium at approximately hour 600. At this point, the total runoff value throughout the watershed begins to level off and oscillate slightly. This oscillation is a result of the same storm being cycled through the model until model reaches equilibrium. The near constant runoff can be interpreted as the base flow of the model domain. For modeling purposes, the results from these base flow runs can be used as the initial conditions for subsequent models.

The team validated the model completion by analyzing the difference between computed and expected water balance for the entire model run. The standard percent difference for this type of model validation is 10^{-3}. Figure 9 shows that the model achieved this at hour 1430.

Table 3. MATLAB Summary Table

Subscript Name	**Description**	**Runtime (Sec)**
Clip_DEM.m	Trim the digital elevation model to the user-defined extent	24.4
Process_DEM.m	Format the DEM into a single column of elevation values with the number of rows and columns defined at the top of the text file	13.2
Convert_DEM.m	convert the matrix origin from WGS to UTM coordinate system	1
Clip_Landcover.m	Trim the landcover raster to the user-defined extent	8.3
landcover_ind.m	Format the landcover raster to a single column, then convert categorical data to a one-hot-encoding format	127.1
extract_nc.m	Extract meteorological forcings to the user-defined spatial and temporal extent, then format to CLM specified format.	16.4
Import_Gleeson.m	Import the Gleeson table, which defines the van Genuchten parameters based on soil type.	4.4
EG_K_{sat}.m	Replace null values in the unburned K_{sat} raster with K_{sat} values from the Gleeson table based on user-defined soil type	22.4
create_variableDZ.m	Calculate the depth of each matrix layer based on user-specified total depth and layers burned.	0.3
Burnscar.m	Replace null values in the unburned K_{sat} raster with K_{sat} values from the Gleeson table based on user-defined soil type. Build a 3-dimensional raster by layering burned matrices over unburned matrices.	42.4
Burnscar_Conversion.m	Format the 3D burnscar matrix into a single column of elevation values with the number of rows and columns defined at the top of the text file	9.5
Create_drv_clmin.m	Create the file necessary to initiate the CLM run	1.5
Indicatorfield.m	Build a 3D indicator field of values that matches the domain size	11.6
Create_TCL.m	Create the file necessary to initiate the ParFlow run	0.3
Total		282.8

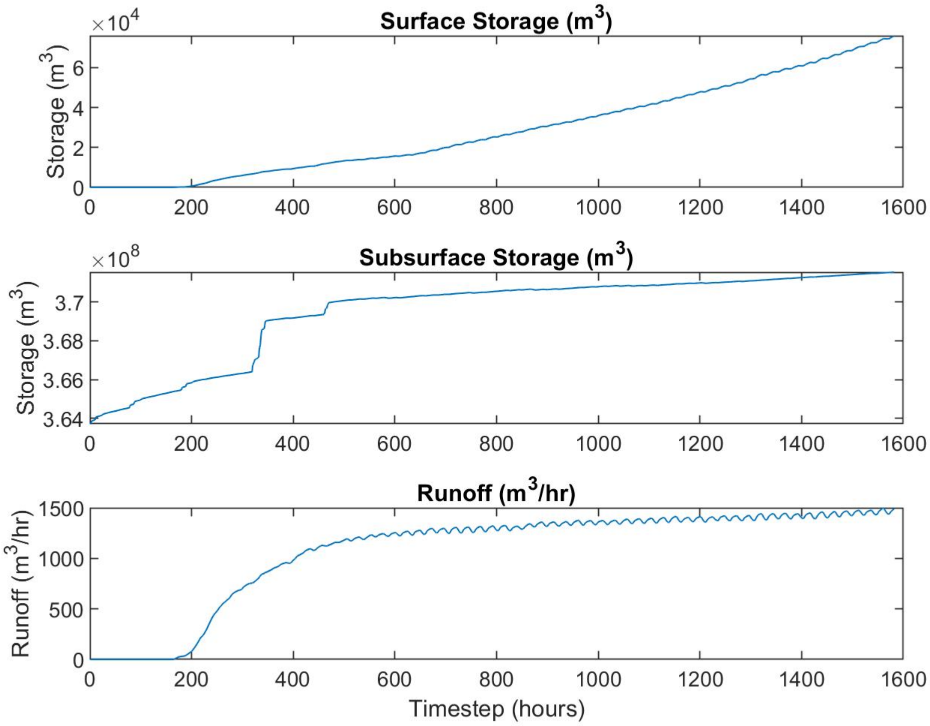

Figure 8. ParFlow Results Graphs

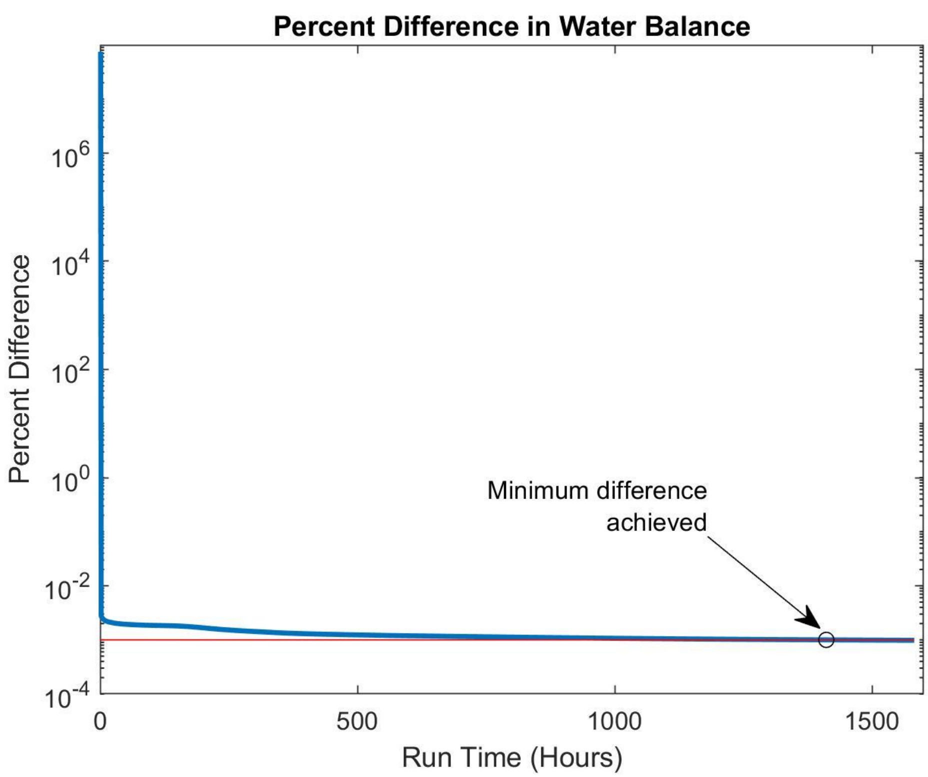

Figure 9. Percent Difference in Expected versus Observed Water Balance

Chapter 4

Conclusion

This work was initially envisioned as a two-phase study where Phase One built the framework. Phase Two used the framework to compare model sensitivity to many parameters and validate against several datasets. Running the sample model to completion proves that this framework is a viable method of initiating ParFlow-CLM models with minimal effort.

For Phase Two, other researchers in the Lopez Water Lab are currently using this framework to run simulations focused on their area of interest. These endeavors include studying hydrophobic layer development and degradation over time and the effect of wildfires on watershed hydrology on a decade-long time scale. Future work by the lab may explore hillslope instability based on pre- and post-fire conditions.

Future development of this framework may include prompts in the user-defined section indicating the minimum and maximum latitude and longitude coordinates available for modeling and a clear definition of the maximum domain size recommended per processor available. The horizontal spatial resolution (30m x 30m) was predetermined by the resolution of the input datasets and is currently not a parameter the user can change, however, updated input datasets may change this in the future. This framework may also advance in reclassifying vegetation types based on burn severity. Currently, the framework only changes the saturated hydraulic conductivity. The model should reflect the amount of vegetation loss by changing the land cover type and using the appropriate leaf area index values based on the available remote sensed data. Hydrophobic layer thickness and position is known to vary over time, so the model should reflect this as well.

REFERENCES

Ashby, S. F., & Falgout, R. D. (1996). A Parallel Multigrid Preconditioned Conjugate Gradient. *124*(1), 145-159.

Atchley, A. L., Kinoshita, A. M., Lopez, S. R., Trader, L., & Middleton, R. (2018). Simulating surface and subsurface water balance changes due to burn severity. *Vadose Zone Journal*, *17*(1), 1-13.

California Department of Water Resources. (2017). *Water Year 2017: What a Difference a Year Makes.* Water Year Report, Sacramento, Ca.

Cannon, S., Boldt, E., Kean, J., Laber, J., & Staley, D. (2010). *Relations between rainfall and postfire debris-flow and flood magnitudes for emergency-response planning, San Gabriel Mountains, southern California.* U.S. Geological Survey.

Cawson, J. G., Nyman, P., Smith, H. G., Lane, P. N., & Sheridan, G. J. (2016). How soil temperatures during prescribed burning affect soil water repellency, infiltration and erosion. *Geoderma*(278), 12-22.

Cawson, J., Sheridan, G., Smith, H., & Lane, P. (2012). Surface runoff and erosion after prescribed burning and the effect of different fire regimes in forests and shrublands: A review. *21*(7), 857-872. doi:10.1071/WF11160

Center for Hydrometerology and Remote Sensing. (2015). *PERSIANN Data Portal*. Retrieved December 2020

Chaparro, D., Vall-Llossera, M., Piles, M., Camps, A., Rüdiger, C., & Riera-Tatché, R. (2016). Predicting the extent of wildfires using remotely sensed soil moisture and temperature trends. *9*(6), 2818-2829.

Condon, L. E., Maxwell, R. M., & Gangopadhyay, S. (2011). The impact of subsurface characterization on regional water budgets in an integrated physical hydrology model of the Upper Klamath Basin. *AGU Fall Meeting Abstracts* (pp. H31F-1235). American Geophysical Union.

Condon, L., & Maxwell, R. (2015). Evaluating the relationship between topography and groundwater using outputs from a continental-scale integrated hydrology model. *Water Resources Research*, 6602-6621.

Crow, W. T., Chen, F., Reichle, H. R., & Xia, Y. (2019). Diagnosing bias in modeled soil moisture/runoff coupling strength using the SMAP Level 4 soil moisture product. (55), 7010-7026. doi:10.1029/2019WR025245

Cydzik, K., & Hogue, T. (2009). Modeling Postfire Response and Recovery using the Hydrologic Engineering Center Hydrologic Modeling System (HEC-HMS). *JAWRA Journal of American Water Resources Association*, *45*(3).

Dai, Y., Zeng, X., Dickinson, R. E., Baker, I., Bonan, G. B., & Bosilovich, M. G. (2003). The common land model. *Bulletin of the American Meteorlogical Society*(84), 1013-1024.

DeBano, L. (1968). Water Movement in Water Repellent Soils. *Symposium on Water Repellent Soils.* Riverside, California: University of California, Riverside.

DeBano, L. (2000). The role of fire and soil heating on water repellency in wildland environments: a review. *Journal of Hydrology*, 195–206.

Ebel, B. (2013). Simulated Unsaturated Flow Processes after Wildfire and Interactions with Slope Aspect. *Water Resources Research*, *49*, 8090-8107.

Ebel, B. A. (2012). Hydrologic Conditions Controlling Runoff Generation Immediately After Wildfire. *Water Resources Research, 48*(3).

Entekhabi, D., Yueh, S., O'Neill, P. E., Kellogg, K. H., Allen, A., Bindlish, R., & Das, N. (2014). *SMAP handbook—Soil Moisture Active Passive: Mapping Soil Moisture and Freeze/Thaw From Space.* Pasadena, California: Jet Propulsion Lab - California Intitute of Technology.

Escobar-Sanchez, I. (2020). *Wildfire Impacts on Hydrologic Components in Southern California using ParFlow-CLM: A Sensitivity Analysis.* California State University, Los Angeles, Department of Civil Engineering. Los Angeles: Proquest Dissertations Publishing.

ESRI. (2011). ArcGIS Pro 2.9.3. Redlands, Ca: Environmental Systems Research Institute .

Fisher, J. B., & team, E. A. (2015). *ECOsystem Spaceborne Thermal Radiometer Experiment on Space Station (ECOSTRESS): Level-3 evapotranspiration LE (ET_PT-JPL) Algorithm Theoretical Basis Document (ATBD).* Pasadena, California: Jet Propulsion Laboratory.

Fisher, J. B., Lee, B., Purdy, A. J., Halverson, G. H., Dohlen, M. B., Cawse-Nicholson, K., & Hook, S. (2020). ECOSTRESS: NASA's next generation mission to measure evapotranspiration from the International Space Station. *56*(4).

Fisher, J. B., Tu, K., & & Baldocchi, D. D. (2008). Global estimates of the land-atmosphere water flux based on monthly AVHRR and ISLSCP-II data, validated at 16 FLUXNET sites. *112*(3), 901-919.

Fox, D. M., Darboux, F., & Carrega, P. (2007). Effects of fire-induced water repellency on soil aggregate stability, splash erosion, and saturated hydraulic conductivity for different size fractions. *Hydrological Processes: An International Journal, 21*(17), 2377-2384.

Friedl, M. A., Strahler, A. H., & Hodges, J. (2010). ISLSCP II MODIS (Collection 4) IGBP Land Cover, 2000-2001. *Oak Ridge National Laboratory Distributed Active Archive Center*.

Gleeson, T., Smith, L., Moosdorf, N., Hartmann, J., Durr, H. H., Manning, A. H., . . . Jellinek, A. (2011). Mapping permeability over the surface of the Earth. *Geophysical Research Papers*.

Hulley, G., Hook, S., Fisher, J., & Lee, C. (2017). ECOSTRESS, A NASA Earth-Ventures Instrument for studying links between the water cycle and plant health over the diurnal cycle. *IEEE International Geoscience and Remote Sensing Symposium (IGARSS)* (pp. 5494-5496). IEEE.

Kauffmann, R. K., Kauppi, H., Mann, M. L., & Stock, J. H. (2011). Reconciling Anthropogenic Climate Change with Observed Temperature 1998-2008. *Proceedings of the National Academy of Sciences, 108*(29), 11790-11793.

Keeley, J. E. (2009). Fire intensity, fire severity and burn severity: a brief review and suggested usage. *18*(1), 116-126.

Kerr, Y. H., Waldteufel, P., Wigneron, J. P., Delwart, S., Cabot, F., Boutin, J., & Juglea, S. E. (2010). The SMOS Mission: New tool for monitoring key elements of the global water cycle. *Proceedures of the IEEE*, *98*(5), 666-687.

Khorshidi, M. S., Dennison, P. E., Nikoo, M. R., AghaKouchak, A., Luce, C. H., & Sadegh, M. (2020). Increasing concurrence of wildfire drivers tripled megafire critical danger days in Southern California between 1982 and 2018. *15*(10).

Kinoshita, A. M., & Hogue, T. S. (2011). Spatial and temporal controls on post-fire hydrologic recovery in Southern California watersheds. *87*(2), 240-252.

Kollet, S. J., & Maxwell, R. M. (2008). Capturing the influence of ground-water dynamics on land surface processes using an integrated, distributed watershed model. *Water Resources Research*, *44*(W02402).

Larsen, I. J., MacDonald, L. H., Brown, E., Rough, D., Welsh, M. J., Pietraszek, J. H., & Schaffrath, K. (2009). Causes of post-fire runoff and erosion: Water repellency, cover, or soil sealing? *73*(4), 1393 - 1407.

Li, J. (2020, October). Geography 5220 - Lecture 7. California State University, Los Angeles.

Li, J. (2020, October). Lab Manual 4 - Working with Satellite Precipitation Data. *Geography 5220*. California State University, Los Angeles.

Li, J. (2020, October). Lab Manual 5 - Evaluate Satellite Precipitation Data. *Geography 5220*. California State University, Los Angeles.

Li, J. (2020, November). Lab Manual 6 - Measuring the impact of drought on Texas reservoirs. *Geography 5220*. California State University, Los Angeles.

Maxwell, R. M. (2013). A terrain-following grid transform and preconditioner for parallel, large-scale, integrated hydrologic modeling. *Advanced Water Resources*(53), 109-117.

Maxwell, R. M., & Kollet, S. J. (2006). Integrated surface-groundwater flow modeling: a free-surface overland flow boundary condition in a parallel groundwater flow model. *29*(7), 945-958.

Maxwell, R. M., & Miller, N. L. (2005). Development of a coupled land surface and groundwater model. *Journal of Hydrometeorology*(6), 233-247.

Maxwell, R., Kollet, S., Condon, L., Smith, S., Woodward, C., Falgout, R., . . . Ashby, S. (2019). *ParFlow User's Manual.* Integrated GroundWater Modeling Center Report.

Miller, J., & Thode, A. (2007). Quantifying burn severity in a heterogeneous landscape with a relative version of the delta Normalized Burn Ratio (dNBR). *Remote Sensing of Environment*, 66-80.

NASA. (2021, May 8). *4 NLDAS: Project Goals*. Retrieved from https://ldas.gsfc.nasa.gov/nldas

NASA. (n.d.). *https://gpm.nasa.gov/data/imerg*. Retrieved 12 13, 2020

NASA. (n.d.). *NASA Land Processes Distributed Active Archive Center*. Retrieved May 2021, from https://ecostress.jpl.nasa.gov/data

North American Land Change Monitoring System. (2015). *CEC.org*. Retrieved from http://www.cec.org/north-american-land-change-monitoring-system/

NRCS, U. (n.d.). *Web Soil Survey*. Retrieved May 2021, from https://websoilsurvey.sc.egov.usda.gov/App/HomePage.htm

Poon, P. K., & Kinoshita, A. M. (2018). Spatial and temporal evapotranspiration trends after wildfire in semi-arid landscapes. *559*, 71 - 83.

Rabin, S. S., Melton, J. R., Lasslop, G., Bachelet, D., Forrest, M., Hantson, S., & Arneth, A. (2017). The Fire Modeling Intercomparison Project (FireMIP), phase 1: experimental and analytical protocols with detailed model descriptions. *10*(3), 1175-1197.

Reichle, R. H., Liu, Q., Koster, R. D., Crow, W. T., De Lannoy, G. J., Kimball, J. S., & Walker, J. P. (2019). Version 4 of the SMAP Level-4 Soil Moisture algorithm and data product. *Journal of Advances in Modeling Earth Systems, 11*(10), 3106-3130.

Rust, A. J., Hogue, T. S., Saxe, S., & McCray, J. (2018). Post-fire water-quality response in the western United States. *27*(3), 203-216.

Schaap, M. G., & Leij, F. J. (1998). Database-related accuracy and uncertainty of pedotransfer functions. *163*(10), 765-779.

Stoof, C. R., Ferreira, A. J., Mol, W., Van den Berg, J., De Kort, A., Drooger, S., & Ritsema, C. J. (2015). Soil surface changes increase runoff and erosion risk after a low–moderate severity fire. (239), 58-67.

Team, C. W., & Rajendra, P. K. (2014). *Climate change 2014: Synthesis report. Contribution of working groups I, II and III to the fifth assessment report of the intergovernmental panel on climate change.* Intergovernmental Panel on Climate Change.

Team, I. F. (2018). *Oroville Dam Spillway Incident.* California Department of Water Resources.

Tompson, A., Ababou, R., & Gelhar, L. (1989). Implementation of of the three-dimensional turning bands random field generator. *25*(10), 2227-2243.

United States Geologic Service. (2018). The National Elevation Dataset. USGS.

USFS. (2018). *Thomas Burned Area Report.* USDA - Forest Service.

USGS. (2020). Burned Area Emergency Response Imagery Support Program.

Wagener, T., & Montanari, A. (2011). Convergence of approaches toward reducing uncertainty in predictions in ungauged basins. *Water Resources Research, 47*(6).

Watershed Emergency Response Team - State of California. (2018). *Woolsey and Hill Fires Watershed Emergency Response Team Final Report* . State of California.

Westerling, A., & Bryant, B. (2006). *Climate change and wildfire in and around California: Fire modeling and loss modeling.*

Woodward, C. S., & Jones, J. E. (2001). Newton–Krylov-multigrid solvers for large-scale, highly heterogeneous, variably saturated flow problems. *24*(7), 763-774.

Xia, Y., Mitchell, K., Ek, M., Cosgrove, B., Sheffield, J., Luo, L., & Lohmann, D. (2012). Continental-scale water and energy flux analysis and validation for North American Land Data Assimilation System project phase 2 (NLDAS-2): 2. Validation of model-simulated streamflow. *117*(D3). doi:10.1029/2011jd016051